Solar Energy Materials & Solar Cells 272 (2024) 112877

Contents lists available at ScienceDirect

Solar Energy Materials and Solar Cells

journal homepage: www.elsevier.com/locate/solmat

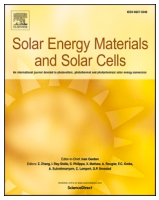

Buyer aware: Three new failure modes in TOPCon modules absent from PERC technology

Chandany Sen *, Haoran Wang, Muhammad Umair Khan, Jiexi Fu, Xinyuan Wu, Xutao Wang, Bram Hoex **

School of Photovoltaic and Renewable Energy Engineering, University of New South Wales, Sydney, NSW, 2052, Australia

ARTICLE INFO

Keywords:
PERC
TOPCon
Modules
Damp heat
Reliability
Failure mode

ABSTRACT

The n-type tunnel oxide passivated contact (TOPCon) technology is going to be the leading industrial technology in 2024. However, there are still concerns about the reliability of TOPCon when used in the field, especially in glass/backsheet modules. This work investigates the impact of damp heat (DH) on the performance TOPCon and PERC glass/backsheet modules by varying bills of materials (BOM), such as polyolefin elastomer (POE), ethyl-vinyl acetate (EVA), and polymer backsheet options. It is found that PERC modules remain stable, with a maximum power loss (P_{max}) of only 1–2%$_{rel}$ after 1000 h of DH testing, regardless of the BOM used. However, TOPCon modules experienced significant degradation with a drop in P_{max} ranging from 4 to 65%$_{rel}$ after the same testing duration. Despite utilizing POE, an expensive encapsulant with a significantly lower water vapour transmission rate than EVA and devoid of acetic acid formation, a severe performance decline was observed in a specific POE variant within TOPCon modules, with a loss of power of up to 65%$_{rel}$. Three types of failures were observed in TOPCon modules: point-localized failure, failure at/around the interconnection of ribbon wires and busbars, and failure throughout the whole area of cells/modules. These failures likely result from electrochemical reactions involving moisture, cell metallization, ribbon wires, contaminants, soldering flux, and additives released from POE. The observed findings underline two crucial points: 1) the vulnerability and potential failure of TOPCon solar cells when exposed to high humidity and contaminants, and 2) the high risk associated with certain POE types, which could potentially adversely affect TOPCon cells. Hence, it is crucial to exercise utmost caution and precision in handling and selecting encapsulation materials for TOPCon modules. Accordingly, urgent and extensive research efforts are crucial to substantially increase our comprehension and fortify the reliability of TOPCon cells against the pernicious effects of moisture and other contaminants.

1. Introduction

Ensuring long-term stability is essential for photovoltaic (PV) systems to minimize the levelized cost of electricity (LCOE). Ideally, a PV system should maintain high-performance levels for 25 to ideally 50 years, with a maximum reduction of 20 % in relative performance, emphasizing the critical importance of long-term stability [1]. Bifacial passivated emitter and rear cell (PERC) dominated the market up to 2024, and tunnel oxide passivated contact (TOPCon) solar cells are expected to become the dominant technology in 2024 [2]. Despite this expected market dominance, TOPCon solar cells still encounter reliability issues, leading to significant power loss under high humidity conditions [3–6]. These concerns need to be addressed as higher degradation rates would potentially make TOPCon inferior to PERC technology in terms of LCOE.

Ethyl-vinyl acetate (EVA) has been found to exhibit a high water vapour transmission rate (WVTR) and hydrolysis of acetic acid during damp heat testing, contributing to severe reliability concerns [3,7–9]. Conversely, polyolefin elastomer (POE) has demonstrated lower WVTR and lacks acetic acid hydrolysis, making it a preferable alternative to EVA for enhancing PV module reliability [7]. Studies by Sommeling et al. have shown that mini modules encapsulated with glass sheets and EVA on both sides (glass/glass modules structure) experienced degradation of up to ~50%$_{rel}$ after 2500 h of damp heat (DH) testing [3]. However, replacing EVA with POE or thermoplastic polyolefins (TPO) gradually improved reliability, reducing the loss to ~1–6%$_{rel}$ over a

* Corresponding author.
** Corresponding author.
E-mail addresses: Chandany.sen@unsw.edu.au (C. Sen), b.hoex@unsw.edu.au (B. Hoex).

https://doi.org/10.1016/j.solmat.2024.112877
Received 17 March 2024; Received in revised form 12 April 2024; Accepted 15 April 2024
Available online 26 April 2024

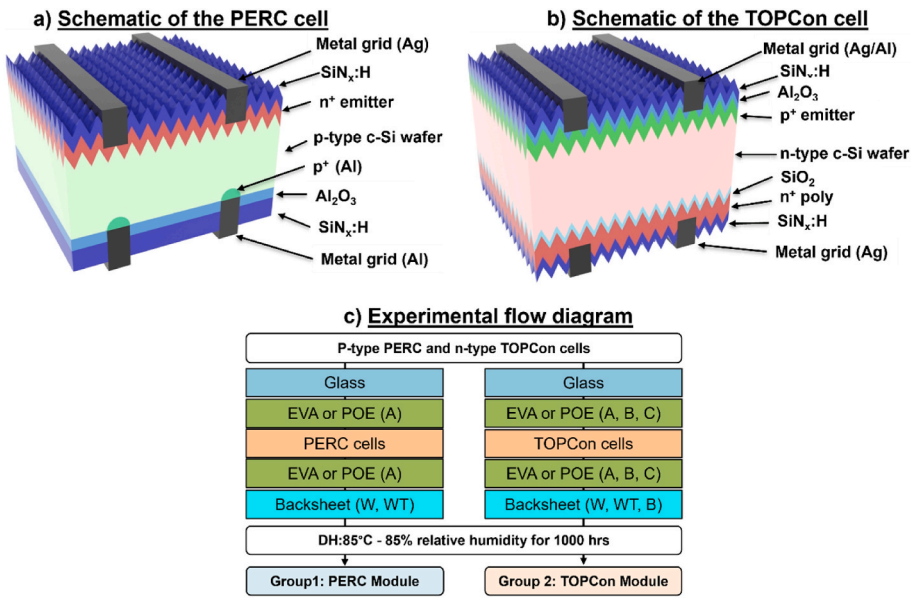

Fig. 1. Schematic of a) PERC cell, b) TOPCon cell and c) the experimental flow diagram used in this work.

similar testing duration. Similarly, Zhou et al. demonstrated that full modules encapsulated with glass sheets and EVA on both sides degraded by over 8.28%$_{rel}$ after 3000 h of DH testing [4]. In contrast, the loss was only ~2%$_{rel}$ when encapsulated with a glass sheet and POE or ethylene-propylene elastomer (EPE) on both sides (glass/glass module structure). However, in the case of glass/backsheet module structures, even when using POE or EPE, a power loss of ~6–7%$_{rel}$ was observed after 2000 h of DH testing. This loss was further mitigated by reducing the cell gap and/or adding an additional metal layer to the rear side. While double-sided glass and POE encapsulation enhance reliability (glass/glass modules structure), they come with drawbacks such as increased risk of damage (e.g., crack or delamination), additional weight (posing challenges for rooftop installation), and higher manufacturing costs [10,11]. A glass-backsheet module with EVA encapsulation remains an attractive option due to affordability, provided it effectively prevents failures induced by humidity or other contaminants. To tackle the issue of humidity-induced degradation in TOPCon cell technologies, comprehensive research is imperative. Therefore, this study aims to investigate the impact of bills of materials (BOM) on the reliability of PERC and TOPCon solar cells.

2. Experiment

Bifacial p-type silicon PERC and n-type TOPCon solar cells sourced from industry were used in this work. The PERC cells featured a phosphorous-doped emitter (n^+ emitter), hydrogenated silicon nitride (SiN_x:H) passivation layer, and screen-printed H-pattern silver grid on the front side. At the rear side, there was an aluminium oxide (Al_2O_3)/SiN_x:H passivation layers stack and a screen-printed H-pattern aluminium grid. The TOPCon cells featured a boron-doped emitter (p^+ emitter), silicon dioxide (SiO_2)/Al_2O_3/SiN_x:H stack, and a screen-printed H-pattern silver grid on the front. At the rear side, there was a SiO_2/phosphorus-doped poly-silicon (n^+poly-Si)/SiN_x:H stack and a screen-printed H-pattern silver grid. Fig. 1 (a) and (b) demonstrate the detailed schematic diagram of PERC and TOPCon cells used in this study, respectively. All cells were soldered on both sides to connect ribbon/tabbing wires to the busbar of cells, creating an 8-cell string. Subsequently, all cells were encapsulated with various BOMs at an industrial facility to create module structures, as listed in Table 1. The encapsulation processes for the modules were executed at the pilot line within the industrial facility. Approximately 30–40 % of the processes were conducted manually, while the remaining processes were automated. These processes included soldering to connect ribbon and

Table 1
Detail module structure and bill of material of PERC and TOPCon used in this study.

(a) Group 1: PERC Modules			
ID	Front side	Cell type	Rear side
(1) P1	Glass/EVA	*p*-typ PERC	EVA/Backsheet type "W"
(2) P2	Glass/POE type "A"	*p*-typ PERC	POE type "A"/Backsheet type "WT"
(3) P3	Glass/POE type "A"	*p*-typ PERC	POE type "A"/Backsheet type "W"
(b) Group 2: TOPCon Modules			
ID	**Front side**	**Cell type**	**Rear side**
(1) T1	Glass/EVA	n-type TOPCon	EVA/Backsheet type "W"
(2) T2	Glass/POE type "A"	n-type TOPCon	POE type "A"/Backsheet type "W"
(3) T3	Glass/POE type "B"	n-type TOPCon	POE type "B"/Backsheet type "WT"
(4) T4	Glass/POE type "B"	n-type TOPCon	POE type "B"/Backsheet type "W"
(5) T5	Glass/POE type "B"	n-type TOPCon	POE type "B"/Backsheet type "B"
(6) T6	Glass/POE type "C"	n-type TOPCon	POE type "C"/Backsheet type "W"
(7) T7	Glass/POE type "C"	n-type TOPCon	POE type "C"/Backsheet type "WT"

Table 2
I–V parameters of PERC modules before (initial) and after 1000 h of damp heat testing.

Initial				
ID	P_{max} (W)	V_{OC} (V)	I_{SC} (A)	R_s (Ω)
P1	29.8	5.56	6.76	0.073
P2	30.0	5.56	6.74	0.067
P3	29.7	5.56	6.73	0.068
DH1000h				
P1	29.5	5.57	6.75	0.076
P2	29.5	5.57	6.71	0.078
P3	29.3	5.56	6.72	0.076

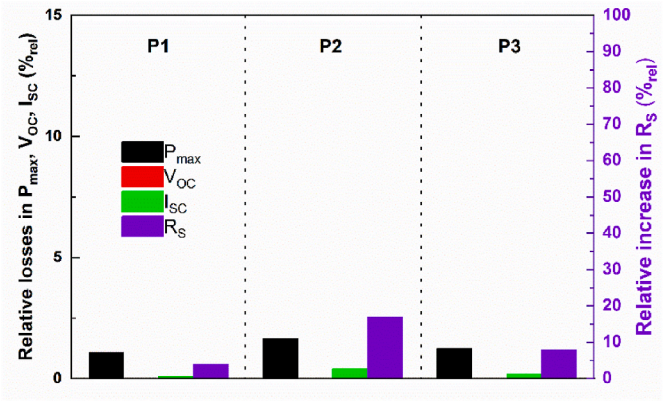

Fig. 2. Relative reduction in P_{max}, V_{OC}, I_{SC} and increase in R_s after 1000 h of damp heat testing of PERC modules.

tabbing wires to the busbars and laminating to join BOM forming modules. All modules underwent DH test at 85 °C and 85 % relative humidity (RH) for up to 1000 h to study humidity-induced failures. Fig. 1 (c) provides a detailed experimental flow diagram in this work. It is worth noting that all BOM components, such as glass, polymer backsheet, EVA, and POE, were procured from various manufacturers worldwide and were considered for high-volume manufacturing. However, specific company names and the details of specific BOMs were excluded due to confidentiality concerns.

For all modules, current-voltage (I–V) measurements were conducted under standard testing conditions before and after 1000 h of DH testing using a commercial module flash tester (Eternalsun Spire, SpiSun Simulator™ 5600SLP Blue System). Line-scan open circuit photoluminescence (PL_{LS}) and electroluminescence (EL_{LS}) images were captured using a BTi-M1 luminescence line-scan system before and after the DH test. Line-scan open circuit PL_{LS} serves as a contactless qualitative method capable of distinguishing series resistance defects from recombination defects in solar cells. The imaging process involves restricting the camera's field of view to a thin line spanning the width of a sample and localizing photoexcitation within this line. Continuous acquisition of individual line images synchronized with sample motion enables real-time imaging. The final image is generated by combining the acquired line images within the sample. Since only a fraction of the cell area is illuminated at any given time, there is a lateral current flow between the illuminated and non-illuminated regions. Consequently, the resulting PL_{LS} intensity is influenced not only by the local minority carrier lifetime but also by the local R_s [12–14]. Regions with relatively high series resistance (R_s) will exhibit a higher PL_{LS} intensity compared to areas with relatively low R_s [12–14].

EL_{LS} image ratios were obtained by dividing EL_{LS} images captured before and after 1000 h of DH testing using LUMITOOLS, an advanced image processing software [15]. Similarly, PL_{LS} image ratios were obtained by i) dividing PL_{LS} images after 1000 h of DH testing by those captured before DH testing (to visualize regions an increase R_s in the modules) and ii) dividing PL_{LS} images taken before (initial) and after 1000 h of DH testing (to visualize regions with an increase in recombination in the module).

3. Results

3.1. PERC modules

Table 2 displays the I–V parameter of PERC modules before and after 1000 h of DH testing. Fig. 2 illustrates the relative losses in maximum power (P_{max}), open circuit voltage (V_{OC}), short circuit current (I_{SC}), and the increase in series resistance (R_s) after 1000 h of DH testing for all PERC modules. The P_{max} of PERC modules degraded by only 1–2%$_{rel}$ (from ~29.8 to ~29.4 W) after 1000 h of DH test. The primary factor contributing to this degradation was an increase in R_s, which rose by ~10%$_{rel}$ (from ~6.9×10^{-2} to ~7.7×10^{-2} Ω). Minimal changes were observed in V_{OC} and I_{SC} (loss below ~0.5%$_{rel}$). Notably, no significant discrepancy in the extent of P_{max} loss was observed with the use of either EVA, POE, or backsheet materials W or WT. This highlights the inherent stability of PERC cells, indicating that both high-quality (POE) and lower-quality (EVA) encapsulation methods have negligible effects on the reliability of PERC cells.

Fig. 3 presents the EL_{LS} images before and after 1000 h of DH testing for PERC modules. The EL_{LS} intensity for modules containing PERC cells

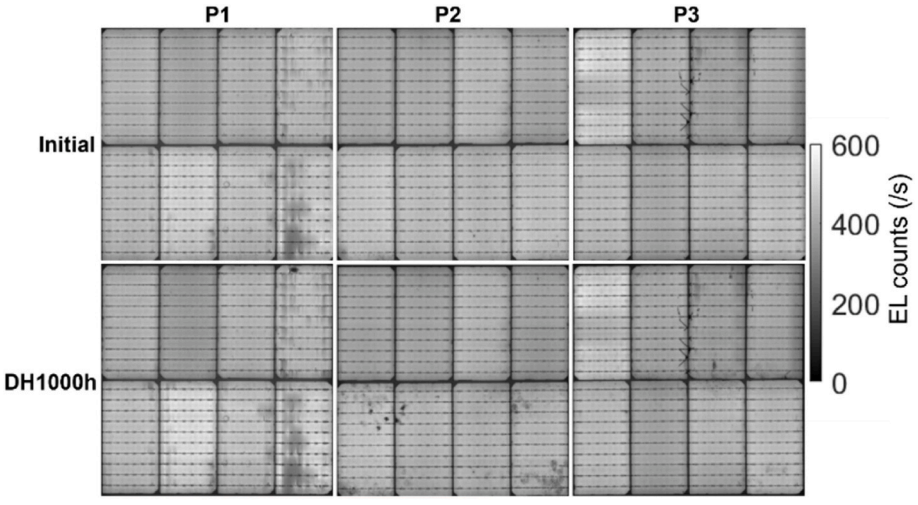

Fig. 3. EL_{LS} images of PERC modules taken before and after 1000 h of damp heat testing.

Table 3
I–V parameters of TOPCon modules before (initial) and after 1000 h of damp heat testing.

ID	T1	T2	T3	T4	T5	T6	T7
Initial							
P_{max} (W)	29.4	30.0	30.6	30.9	29.3	30.5	30.5
V_{OC} (V)	5.76	5.77	5.78	5.79	5.74	5.76	5.77
I_{SC} (A)	6.71	6.71	6.71	6.69	6.38	6.58	6.63
R_S (Ω)	0.072	0.070	0.074	0.072	0.071	0.070	0.073
DH1000h							
P_{max} (W)	26.2	25.3	29.0	29.0	28.3	14.2	10.7
V_{OC} (V)	5.77	5.76	5.78	5.79	5.75	5.75	5.75
I_{SC} (A)	6.67	6.66	6.69	6.66	6.38	5.91	5.15
R_S (Ω)	0.112	0.098	0.095	0.099	0.090	0.345	0.533

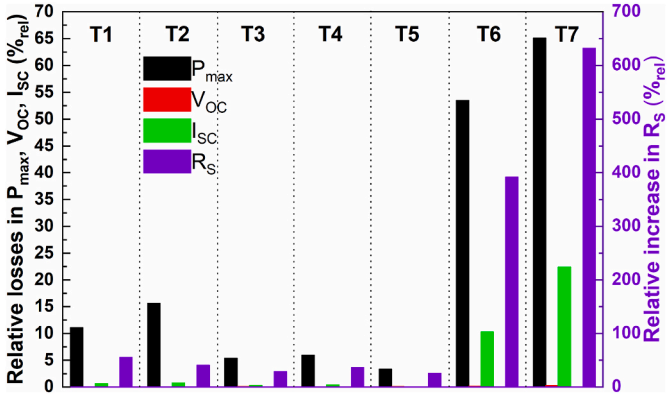

Fig. 4. Relative reduction in P_{max}, V_{OC}, $I_{SC,}$ and increase in R_s of TOPCon modules after 1000 h of damp heat testing.

remained largely unchanged before and after 1000 h of DH testing. Any observed alterations were minimal in nature. These findings were consistent with data obtained through the I–V tester, indicating no significant alteration in both P_{max} and R_s for the modules within the PERC group.

3.2. TOPCon modules

Table 3 shows I–V parameters of TOPCon modules before and after 1000 h of DH testing. Meanwhile, Fig. 4 depicts the relative losses in P_{max}, V_{OC}, I_{SC}, and the increase in R_s of TOPCon modules after 1000 h of DH testing. In contrast to PERC modules, there was a notable decrease in P_{max} observed in TOPCon modules, ranging from 4%$_{rel}$ to 65%$_{rel}$. Modules with POE-B (T3, T4, T5) experienced a reduction in P_{max} of 4–6%$_{rel}$ (P_{max} decreased from ~30.3 to ~28.8 W), while the module with POE-A (T2) exhibited a decrease of ~16%$_{rel}$ (P_{max} decreased from ~30.0 to ~25.3 W) after 1000 h of DH testing. The P_{max} of the module with EVA (T1) degraded ~11%$_{rel}$ (P_{max} decreased from ~29.4 to ~26.2 W). The most significant loss was observed in the module with POE-C (T6, T7), where P_{max} dropped by ~50–65%$_{rel}$ (P_{max} declined from ~30.5 to ~10.7 W). No clear trend was observed when altering the type of polymer backsheet, whether type W, WT, or B. The loss in all modules was primarily attributed to a considerable increase in R_s, which increased by ~25.6–632%$_{rel}$ (absolute R_s increased from ~7.2×10^{-2} to ~53×10^{-2} Ω). V_{OC} and I_{SC} remained relatively stable, with losses below 0.7%$_{rel}$. It is worth noting that the substantial loss in I_{SC}, ~10%$_{rel}$ and ~20%$_{rel}$ observed in the T6 and T7 modules, respectively, was likely attributable to the very high R_s, which impeded carrier collection in these modules. The significant reduction in I_{SC} resulting from poor R_s has been a recurrent observation in our previous studies [16,17].

Figs. 5–7 present the EL_{LS} and EL_{LS} image ratio, and Figs. 8 and 9 show the PL_{LS} images of all TOPCon modules, which displays the specific failure modes of each module. The EL_{LS} counts in TOCPon modules significantly decreased, while the PL_{LS} counts in most modules increased after DH testing. The decrease in the EL_{LS} counts of each module can be better visualized in the EL_{LS} image ratio, as shown in Fig. 5 (c), 6 (c), and 7 (c). This result suggests that the decrease in EL_{LS} intensity observed in TOPCon modules was due to an increase in R_s [13,14]. These results align well with the changes in I–V parameters shown in Fig. 4. It is important to emphasize that the selection of colour for EL/PL imaging was made to facilitate quick interpretation of both failed and non-failed areas within the modules. Typically, we opt for a grayscale colour scale for EL and PL images, a choice based on the familiarity of PV manufacturers, installers and end users with this scheme. This familiarity enables them to swiftly identify any module issues during image review

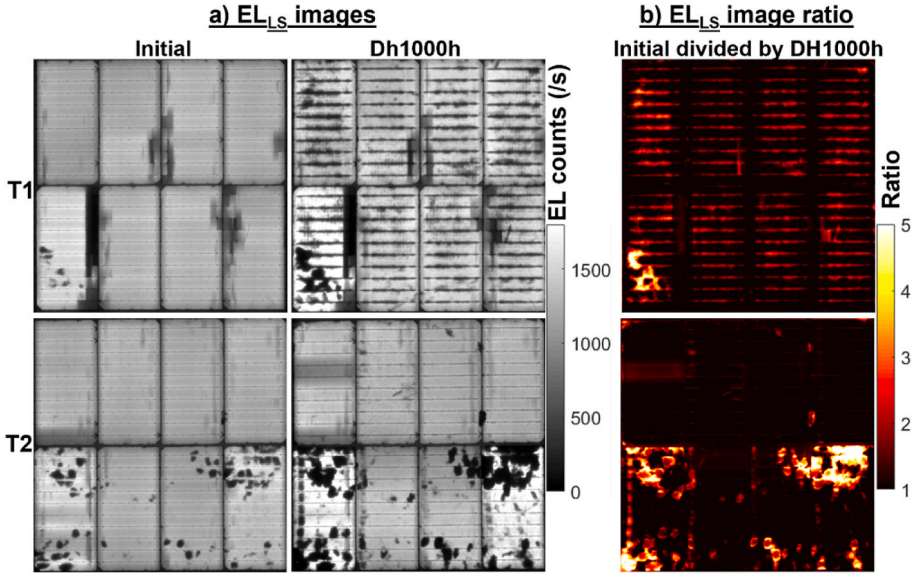

Fig. 5. a) EL_{LS} images of TOPCon modules with EVA_backsheet W (**T1**) and POE-A_backsheet W (**T2**) taken before and after 1000 h of damp heat testing complemented by b) EL_{LS} image ratio images (calculated by dividing the EL_{LS} image at the initial stage by the EL_{LS} image at the DH1000h stage).

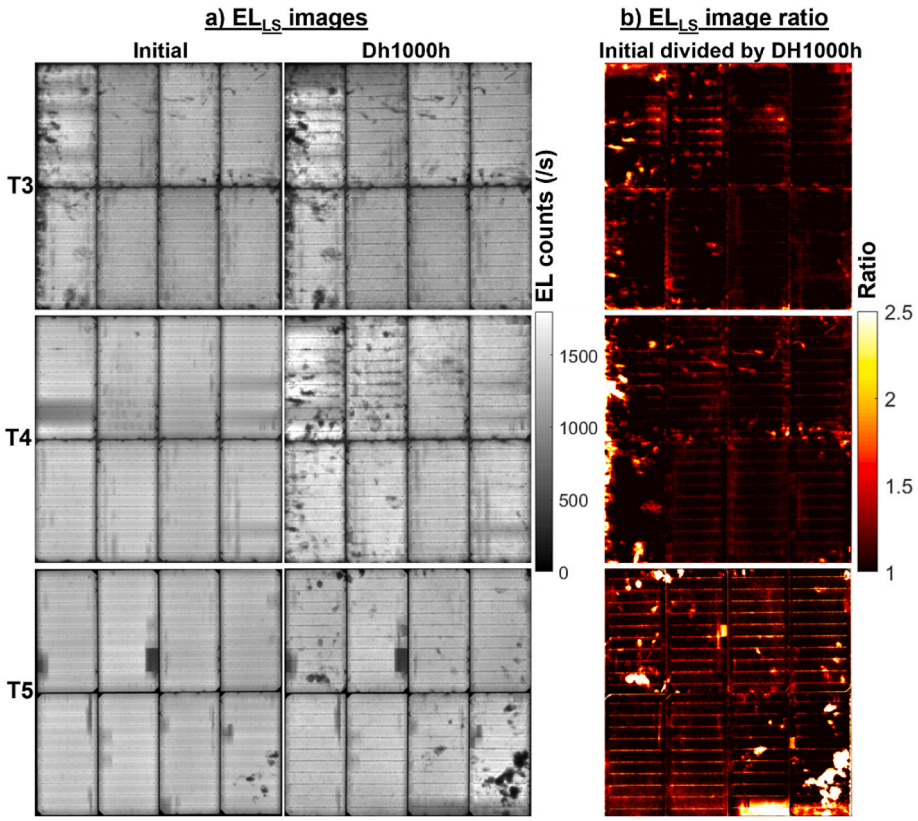

Fig. 6. a) EL_{LS} images taken before and after 1000 h of damp heat testing, and b) EL_{LS} image ratio (calculated by dividing the EL_{LS} image at the initial stage by the EL_{LS} image at the DH1000h stage) of TOPCon modules with POE-B_backsheet WT (**T3**), POE-B_backsheet W (**T4**), POE-B_backsheet B (**T5**).

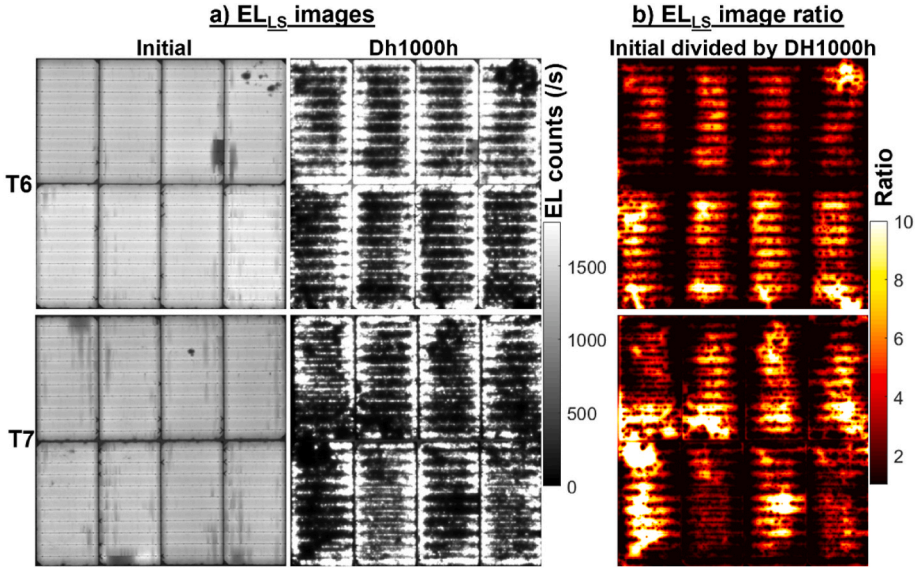

Fig. 7. a) EL_{LS} images taken before and after 1000 h of damp heat testing, and b) EL_{LS} image ratio (calculated by dividing the EL_{LS} image at the initial stage by the EL_{LS} image at the DH1000h stage) of TOPCon modules with POE-C_backsheet W (**T6**) and POE-C_backsheet W (**T7**).

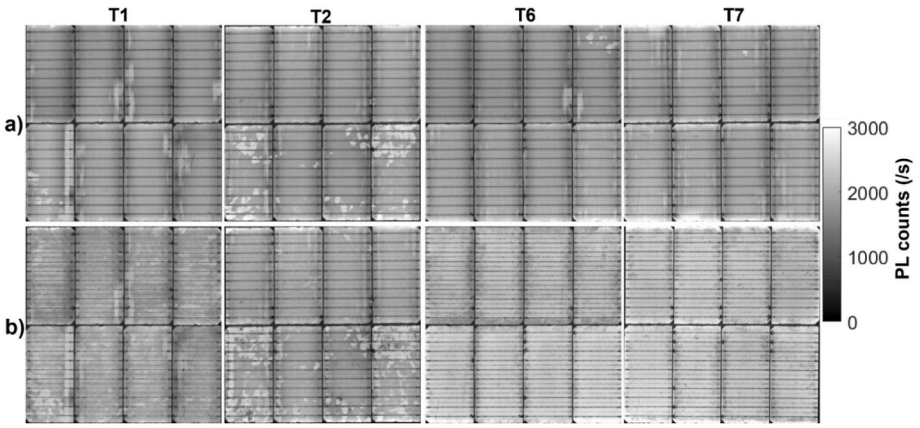

Fig. 8. PL_{LS} images taken before (a) and (b) after 1000 h of damp heat testing of TOPCon modules with EVA_backsheet W (**T1**), POE-A_backsheet W (**T2**), POE-C_backsheet W (**T6**) and POE-C_backsheet WT (**T7**).

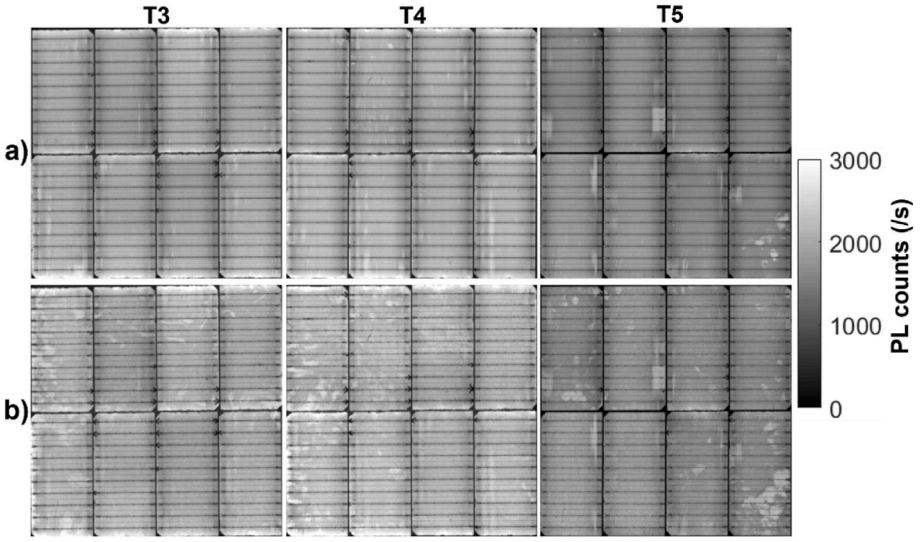

Fig. 9. PL_{LS} image taken before (a) and (b) after 1000 h of damp heat testing of TOPCon modules with POE-B_backsheet WT (**T3**), POE-B_backsheet W (**T4**), and POE-B_backsheet B (**T5**).

without the need for extensive explanation. However, when dealing with image ratios, the use of grayscale can sometimes obscure localized issues, making them more challenging to discern. Hence, we prefer to employ a "hot colour" scale in such cases, as it effectively highlights module issues, thereby facilitating rapid interpretation of the results.

4. Discussion

Overall, we found three distinct failure modes in TOPCon modules, which were notably absent in the PERC modules. The first type of failure mode, Type-1, was a point-localized failure. The second type, Type-2, was a failure mode that occurs at/around the interconnection point between ribbon wires and busbars of the cells. The third type of failure mode, Type-3, was a complete failure across the entire area of the cells/modules.

The Type-1 failure mode, characterized by point-localized issues, was already prevalent in nearly all modules containing TOPCon cells prior to undergoing the DH test (T1-T3, T5, T6). This was evident through a localised low EL intensity and manifested as dark dots randomly distributed within the modules, as depicted in Fig. 5 (a), 6 (a), and 7 (a). In PL_{LS} images, this failure mode appeared as a bright dot pattern randomly scattered within the modules (see Figs. 8 and 9), indicating a loss in R_s within the TOPCon modules. Following 1000 h of DH testing, the majority of these failures had intensified, particularly noticeable in T1 (module with EVA), T2 (module with POE-A), T5 (module with POE-B), and T6 (module with POE-C) samples. This was evidenced by a further decline in EL intensity, prominently observed in Fig. 5 (b), 6 (b), and 7 (b). The exacerbated failure was distinctly visible in the EL_{LS} image ratio images, characterized by bright contrast [refer to Figs. 5(c), 6(c) and 7(c)]. This localized failure led to a substantial drop in EL counts, ranging approximately from $125\%_{rel}$ to $400\%_{rel}$, as illustrated in the EL_{LS} image ratio depicted in Fig. 5 (c), 6 (c), and 7 (c). In one particular module (T2), this failure mode was observed to induce both an increase in R_s and a slight rise in recombination loss. Fig. 10 presents EL_{LS} and PL_{LS} images taken before and after 1000 h of DH testing, along with the PL_{LS} image ratios comparing the DH1000h stage to the initial stage (highlighting areas with increased R_s) and the initial stage to DH1000h stage (highlighting areas with a slight recombination increase) [13,14]. It is worth noting that some of these images were previously displayed in Figs. 5 and 8. This observation is consistent with the I–V data illustrated in Fig. 4, where the I_{SC} of the T2 module slightly declined $\sim 0.75\%_{rel}$ after 1000 h of DH testing.

The specific contaminant responsible for the Type-1 failure mode in TOPCon modules remains unclear at present. A study is currently underway to ascertain the root cause of these failures; however, it is important to note that this investigation is in its early stages, and a

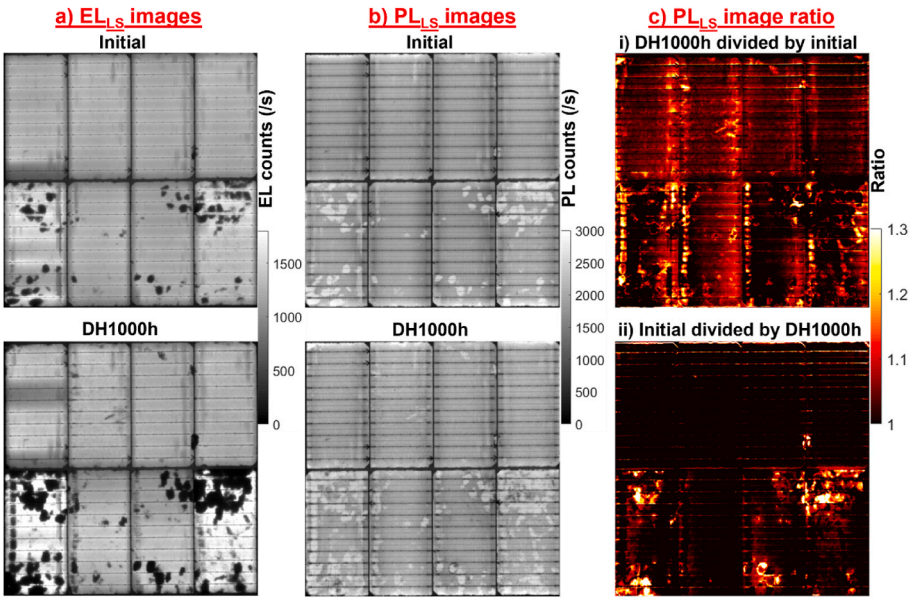

Fig. 10. a) EL_{LS} and b) PL_{LS} images before (initial) and after 1000 h of DH testing, and c) PL_{LS} image ratios of T2 TOPCon module (module with POE-B). The PL_{LS} image ratio was calculated by dividing: i) the PL_{LS} image at the DH1000h stage by the PL_{LS} image at the initial stage and ii) the PL_{LS} image at the initial stage by the PL_{LS} image at DH1000h. In image (i), the bright region indicates areas with increased R_s after 1000 h of DH testing (increase in PL_{LS} intensity after DH testing). Conversely, in image (ii), the bright region highlights areas with recombination increase after 1000 h of DH testing (decrease in PL_{LS} intensity after DH testing).

considerable amount of work remains to be done before definitive conclusions can be reached and they will be shared with the community at a later date. However, it is plausible that sodium (Na) and chlorine (Cl) are implicated in this phenomenon. It has been reported that human fingerprints often contain notable quantities of Na and Cl, posing a risk of solar cell contamination during production if not managed meticulously [18,19]. Previous investigations have demonstrated the significant impact of NaCl on various cell technologies [6,20–22]. Notably, TOPCon cells were found to be particularly vulnerable, while PERC cells exhibited less susceptibility [6]. It was observed that NaCl could induce rapid corrosion of the front contact in TOPCon cells, potentially leading to an increase in R_s, resulting in relative P_{max} loss of up to 70 % within just 20 h of DH testing in non-encapsulated cells [6].

In this study, it is plausible that NaCl might have been accidently introduced to the cells during handling or storage, possibly by gloves contaminated by direct contact with bare hands or placement of cells in an inadequately controlled environment prior to encapsulation. However, owing to the heightened sensitivity of the metallization in TOPCon cells to NaCl compared to PERC cells, as evidenced in previous research, the failure was more pronounced in modules containing TOPCon cells versus PERC cells [6]. Moreover, it is plausible that the localized failure observed in the TOPCon module was exacerbated by the residue of soldering flux used during the connection of ribbon wires and busbars of the cells. Previous studies have indicated that the residue of certain types of soldering flux can induce metal corrosion, thereby increasing the R_s of solar cells after DH testing [16,23]. During the handling and soldering processes involved in connecting ribbon wires to busbars before encapsulation, this flux may inadvertently infiltrate the TOPCon cells, resulting in an increase in R_s. Further elucidation on the potential role of soldering flux in precipitating TOPCon module failure will be revisited in the subsequent section.

It's notable that a comparable localized failure, identified as Type-1 failure mode, was also observed in single glass modules featuring silicon heterojunction (HJT) solar cells in our previous research [16]. This failure mode led to a P_{max} loss of up to 40%$_{rel}$ after 4000 h of DH testing. Despite the modules in our earlier study being fabricated by a different industry partner from those used in this investigation, intriguingly, similar failure patterns emerged. However, in modules containing HJT cells, these contaminants resulted in more pronounced recombination losses (V_{OC} and I_{SC} reduction) rather than an increase in R_s. This underscores the possibility of similar contaminants occurring in numerous industrial settings, emphasizing the need to mitigate their adverse effects during DH testing, especially when dealing with TOPCon and HJT cells.

Type-2 failure mode refers to failures occurring at or around the interconnection points between ribbon wires and busbars of the cells. This failure initiates at these interconnection points and gradually extends to the surrounding cell areas with prolonged DH testing. This failure mode is more prominently observed in T3 (modules with POE-B, Backsheet WT), T4 (modules with POE-B, Backsheet W), and T5 (modules with POE-B, Backsheet B), with a particularly pronounced presence in T1 (modules with EVA). This failure mode has been observed to induce an increase in R_s in certain modules (T3, T4, T5). Additionally, in some instances, this failure mode has been noted to cause both an increase in R_s and a slight increase in recombination. An illustrative example of this can be seen in T1 (modules with EVA, Backsheet W), as presented in Fig. 11. Fig. 11 displays EL_{LS} and PL_{LS} images captured before and after 1000 h of DH testing, along with the PL_{LS} image ratios comparing the DH1000h stage to the initial stage (highlighting areas with increased R_s) and the initial stage to DH1000h stage (highlighting areas with a slight recombination increase) [13,14]. This result aligned with the I–V data presented in Fig. 4, where a minor decrease in I_{SC} (~0.5%$_{rel}$) was observed in the T1 module after 1000 h of DH testing (see Fig. 12).

The Type-2 failure mode has also been observed in the works of Zhou et al. and by Hangzhou First, where it was observed in nearly every glass/backsheet module encapsulated with either EVA, EPE, or POE [4,5]. Furthermore, our previous research on HJT glass backsheet modules (Type-2 and Type-4 failure modes) has also identified this particular failure mode [16]. The occurrence of this failure may be attributed to a chemical reaction involving ribbon wires, cell metallization, moisture, and soldering flux [23]. This reaction can take place with [16,24] or without [23] the presence of acetic acid, which is typically generated by hydrolysis from EVA. This scenario is evident in the T3 module (equipped with POE-B) as well as in modules T6 and T7 (utilizing POE-C), as will be demonstrated in Fig. 12 (showing EL_{LS} images after 500 h of DH testing). Additionally, this issue was observed by Hangzhou First involving modules with POE, a material not known to produce acetic acid [5].

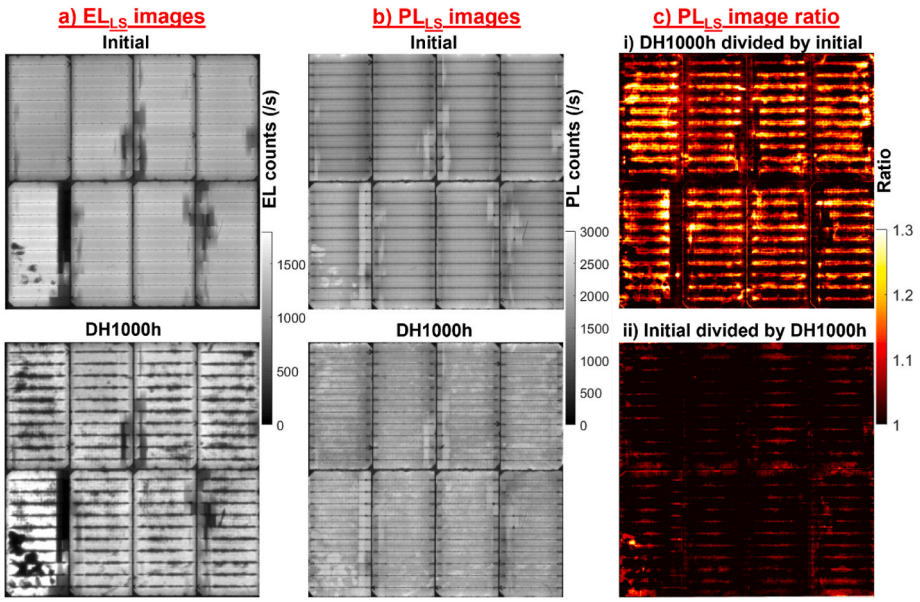

Fig. 11. a) EL_{LS} and b) PL_{LS} images before (initial) and after 1000 h of DH testing, c) PL_{LS} image ratios of T1 TOPCon module (module with EVA). The PL_{LS} image ratio was calculated by dividing i) the PL_{LS} image at the DH1000h stage by the PL_{LS} image at the initial stage and ii) the PL_{LS} image at the initial stage by the PL_{LS} image at DH1000h. In image (i), the bright region indicates areas with increased R_s after 1000 h of DH testing (increase in PL_{LS} intensity after DH testing). Conversely, in image (ii), the bright region highlights areas with recombination increase after 1000 h of DH testing (decrease in PL_{LS} intensity after DH testing).

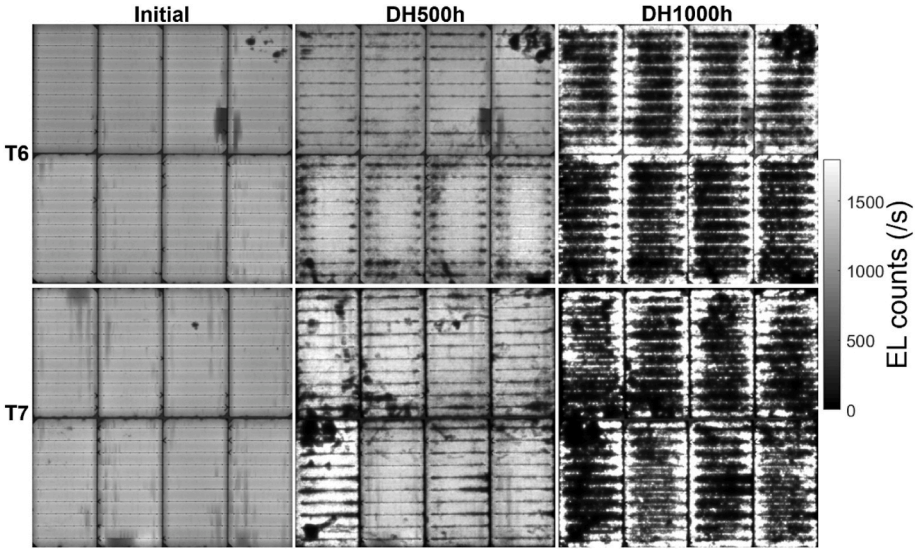

Fig. 12. EL_{LS} image taken before and after 500 h and 1000 h of damp heat testing of T6 and T7 TOPCon modules (module with POE-C), showing the gradual transition from Type-2 failure mode to Type-3 failure mode following prolonged DH testing.

The Type-3 failure mode, characterized by failure across the entire module area, was notably more prominent in the T6 and T7 modules (modules with POE-C). This failure mode emerges from a prolonged manifestation of the Type-2 failure mode, as demonstrated in Fig. 12. The evolution of EL_{LS} images at different stages of DH testing (initial, 500 h, and 1000 h) is depicted in Fig. 12 (note that some images were previously shown in Fig. 7). Type-2 failure mode was observed in these modules after 500 h of DH testing, progressing subsequently into Type-3 failure mode after 1000 h of DH testing. This particular failure mode has also been observed previously in HJT modules encapsulated with a front glass sheet, EVA, and polymer backsheet (referred to as Type-3 failure mode), resulting in up to a 50%$_{rel}$ P_{max} loss after 2500 h of DH testing [16]. The precise root cause of this failure mode remains unknown, and ongoing research aims to determine its underlying factors. However, it is plausible that this failure could be attributed to the electrochemical reaction between cell metallization, moisture, and soldering flux [16, 23] and potentially exacerbated by critical elements released from the POE-C. It remains uncertain why POE-C exhibited a significantly negative impact on TOPCon cells compared to POE-A and POE-B and why there is a variance in chemical composition between these materials. This discrepancy resulted in a more extensive failure, even surpassing that of cheaper encapsulation materials like EVA (P_{max} drop of ~11%$_{rel}$). Studies are underway to analyse the critical composition and additives of each POE encapsulation to ascertain if they contribute to causing this severe failure, as observed in T6 and T7. It is important to note that the Type-3 failure mode presented in this study has also been observed by another industry partner (who conducted separate testing at their facility) when utilizing a specific type of POE (distinct from POE-C used in this study), although the data are not disclosed here due to confidentiality reasons. These findings underscore the critical issue

associated with certain types of POE encapsulations and suggest that greater attention and detailed study should be exercised before selecting the type of encapsulation for TOPCon cells.

5. Conclusion

In summary, this study delves into the effects of damp heat-induced degradation in bifacial n-type TOPCon and p-type PERC glass backsheet modules, employing various BOMs such as POE, EVA, and different backsheet options. Our findings indicate that PERC modules demonstrate stability, with only a 1–2%$_{rel}$ decrease in P_{max} after 1000 h of DH testing, irrespective of the BOM used. Conversely, TOPCon modules experience significant degradation, with P_{max} decreasing by 4–65%$_{rel}$ relative after the same DH testing duration. Despite utilizing POE, an expensive encapsulant type with a significantly lower water vapour transmission rate and the absence of acetic acid formation, a substantial performance decrease was observed in modules with POE-C (P_{max} drop ~65%$_{rel}$) compared to modules with EVA, where the P_{max} drop was only ~11%$_{rel}$. Across all modules, this loss is primarily due to a severe increase in R_s. Three types of failure modes are observed in TOPCon modules: point-localized failure (Type-1), failure at/around the interconnection of ribbon wires and busbars (Type-2), and failure throughout the entire area of cells/modules (Type-3). Type-1 failure could be attributed to the electrochemical reaction between moisture, cell metallization, and contaminants likely present on the cells before encapsulation. Type-2 failure mode was observed in modules with TOPCon cells encapsulated with either EVA or POE, starting at the interconnection point and then spreading to the surrounding cell area after extended DH testing. This failure mode likely results from an electrochemical reaction between moisture, ribbon wires, cell metallization, and soldering flux with or without acetic acid, causing metal corrosion and an increase in R_s. Type-3 failure mode occurred mainly in modules with TOPCon modules encapsulated with POE-C, likely due to an electrochemical reaction between cell metallization, moisture, soldering flux, and critical elements released from the POE-C, leading to a severe increase in R_s and a significant P_{max} drop. These findings highlight two critical points: firstly, the vulnerability and potential failure of TOPCon solar cells when exposed to high humidity and contaminants before encapsulation, and secondly, the high risk associated with certain POE types, which could adversely affect TOPCon cells. Hence, careful consideration is necessary when handling and selecting encapsulants for TOPCon modules. Consequently, further research is essential to deepen understanding and enhance the reliability of TOPCon cells against the deleterious effects of moisture and contaminants, particularly when a glass/backsheet module structure is utilized.

CRediT authorship contribution statement

Chandany Sen: Writing – review & editing, Writing – original draft, Validation, Methodology, Investigation, Formal analysis, Conceptualization. **Haoran Wang:** Methodology, Investigation. **Muhammad Umair Khan:** Resources, Investigation, Data curation. **Jiexi Fu:** Investigation, Data curation. **Xinyuan Wu:** Visualization, Methodology, Data curation. **Xutao Wang:** Investigation, Data curation. **Bram Hoex:** Writing – review & editing, Validation, Supervision, Resources, Project administration, Conceptualization.

Declaration of competing interest

The authors declare that they have no known competing financial interests or personal relationships that could have appeared to influence the work reported in this paper.

Data availability

Data will be made available on request.

Acknowledgements

This work was supported by the Australian Government through the Australian Renewable Energy.

Agency (ARENA 1–060 Extension project) and the Australian Centre for Advanced Photovoltaics (ACAP) also funded by ARENA. The responsibility for the views, information, or advice expressed herein is not accepted by the Australian Government. The authors extend their gratitude to The LDOT team at SPREE UNSW, both at TETB and SIRF, for their invaluable support in upholding health and safety standards within the lab and ensuring the seamless operation of the facility, which facilitated the progress of our work.

References

[1] I.M. Peters, J. Hauch, C. Brabec, P. Sinha, The value of stability in photovoltaics, Joule 5 (2021) 3137–3153, https://doi.org/10.1016/j.joule.2021.10.019.
[2] International Technology Roadmap for Photovoltaic, ITRPV 14. Edition (2023).
[3] P.M. Sommeling, J. Liu, J.M. Kroon, Corrosion effects in bifacial crystalline silicon PV modules; interactions between metallization and encapsulation, Sol. Energy Mater. Sol. Cell. 256 (2023), https://doi.org/10.1016/j.solmat.2023.112321.
[4] Y. Zhou, D. Chen, Y. Ye, H. Yin, X. Niu, Damp-heat endurance investigation of PV modules based on n-type bifacial passivated contact cells, in: 40th European Photovoltaic Solar Energy Conference and Exhibition, 2023, https://doi.org/10.4229/EUPVSEC2023/3AV.2.41.
[5] R. Sengupta, Hangzhou First's New Encapsulation Solutions Address Challenges in N-TOPcon Technology, Taiyangnews, 2024. https://taiyangnews.info/hangzhou-firsts-new-encapsulation-solutions-address-challenges-in-n-topcon-technology/. (Accessed 24 February 2024).
[6] C. Sen, X. Wu, H. Wang, M.U. Khan, L. Mao, F. Jiang, T. Xu, G. Zhang, C. Chan, B. Hoex, Accelerated damp-heat testing at the cell-level of bifacial silicon HJT, PERC and TOPCon solar cells using sodium chloride, Sol. Energy Mater. Sol. Cell. 262 (2023) 112554, https://doi.org/10.1016/j.solmat.2023.112554.
[7] Y. Bai, Y. Zhao, J. Li, H. Chen, A. Lambertz, Q. Qiu, C. Qian, J. Shi, W. Liu, T. Chen, J. Yu, K. Ding, J. Yu, Lower levelized cost of Energy Achievement of silicon heterojunction solar modules with low water vapor transmission rate encapsulants, Energy Technol. 11 (2023), https://doi.org/10.1002/ente.202201466.
[8] M.D. Kempe, G.J. Jorgensen, K.M. Terwilliger, T.J. McMahon, C.E. Kennedy, T. T. Borek, Acetic acid production and glass transition concerns with ethylene-vinyl acetate used in photovoltaic devices, Sol. Energy Mater. Sol. Cell. 91 (2007) 315–329, https://doi.org/10.1016/j.solmat.2006.10.009.
[9] A.W. Czanderna, Encapsulation of PV Modules Using Ethylene Vinyl Acetate Copolymer as a Pottant: A Critical Review, 1996.
[10] M. Hutchins, The weekend read: bifacial drives PV encapsulant switch, Pv Magazine International (2021). https://www.pv-magazine.com/2021/03/20/the-weekend-read-bifacial-drives-pv-encapsulant-switch/. (Accessed 18 March 2024).
[11] JinkoSolar: Transparent backsheet vs dual glass—Advantages and disadvantages, PV Tech. https://www.pv-tech.org/industry-updates/jinkosolar-transparent-backsheet-vs-dual-glass-advantages-and-disadvantages/, 2020. (Accessed 18 July 2023).
[12] M. Kasemann, L.M. Reindl, B. Michl, W. Warta, A. Schütt, J. Carstensen, Contactless qualitative series resistance imaging on solar cells, IEEE J Photovolt 2 (2012) 181–183, https://doi.org/10.1109/JPHOTOV.2012.2184524.
[13] I. Zafirovska, M.K. Juhl, J.W. Weber, J. Wong, T. Trupke, Detection of finger Interruptions in silicon solar cells using line scan photoluminescence imaging, IEEE J Photovolt 7 (2017) 1496–1502, https://doi.org/10.1109/JPHOTOV.2017.2732220.
[14] I. Zafirovska, M.K. Juhl, T. Trupke, Comparison of line scan luminescence imaging Techniques for defect Characterisation in crystalline silicon solar modules. 2018 IEEE 7th World Conference on Photovoltaic Energy Conversion (WCPEC)(A Joint Conference of 45th IEEE PVSC, 28th PVSEC & 34th EU PVSEC), 2018, pp. 1364–1369.
[15] D.N.R. Payne, C. Vargas, Z. Hameiri, S.R. Wenham, D.M. Bagnall, An advanced software suite for the processing and analysis of silicon luminescence images, Comput. Phys. Commun. 215 (2017) 223–234, https://doi.org/10.1016/j.cpc.2017.02.012.
[16] C. Sen, H. Wang, X. Wu, M.U. Khan, C. Chan, M. Abbott, B. Hoex, Four failure modes in silicon heterojunction glass-backsheet modules, Sol. Energy Mater. Sol. Cell. 257 (2023) 112358, https://doi.org/10.1016/j.solmat.2023.112358.
[17] C. Sen, X. Wu, H. Wang, M.U. Khan, L. Mao, F. Jiang, T. Xu, G. Zhang, C. Chan, B. Hoex, Accelerated damp-heat testing at the cell-level of bifacial silicon HJT, PERC and TOPCon solar cells using sodium chloride, Sol. Energy Mater. Sol. Cell. (2023).
[18] M. Wilson, A. Savtchouk, P. Edelman, D. Marinskiy, J. Lagowski, Drift characteristics of mobile ions in SiNx films and solar cells, Sol. Energy Mater. Sol. Cell. 142 (2015) 102–106, https://doi.org/10.1016/j.solmat.2015.06.022.
[19] C.G. Worley, S.S. Wiltshire, T.C. Miller, G.J. Havrilla, V. Majidi, Detection of visible and latent fingerprints using micro-X-ray fluorescence elemental imaging, J. Forensic Sci. 51 (2006) 57–63, https://doi.org/10.1111/j.1556-4029.2005.00006.x.
[20] X. Wu, C. Sen, H. Wang, X. Wang, Y. Wu, M.U. Khan, L. Mao, F. Jiang, T. Xu, G. Zhang, B. Hoex, Addressing sodium ion-related degradation in SHJ cells by the

application of nano-scale barrier layers, Sol. Energy Mater. Sol. Cell. 264 (2024) 112604, https://doi.org/10.1016/j.solmat.2023.112604.
[21] C. Sen, C. Chan, X. Wu, H. Wang, M.U. Khan, L. Mao, J.-N. Jaubert, F. Jiang, G. Zhang, B. Hoex, The role of Na + contamination in humidity-induced degradation in silicon HJT cells, in: Asia-Pacific Solar Research Conference, 2022.
[22] M.U. Khan, C. Sen, C. Chan, M. Abbott, G. Poduval, Y. Wu, R. Lv, G. Zhang, B. Hoex, Supercharging cell-level potential-induced degradation (PID) testing using a salt-enriched hybrid polymer layer, Sol. Energy Mater. Sol. Cell. 260 (2023) 112479, https://doi.org/10.1016/j.solmat.2023.112479.
[23] Y. Ino, S. Asao, K. Shirasawa, H. Takato, Effect of soldering on the module degradation along bus bar in DH test and PCT for crystalline Si PV modules. 2018 IEEE 7th World Conference on Photovoltaic Energy Conversion (WCPEC)(A Joint Conference of 45th IEEE PVSC, 28th PVSEC & 34th EU PVSEC), 2018, pp. 3552–3557, https://doi.org/10.1109/PVSC.2018.8548219.
[24] N. Iqbal, D.J. Colvin, E.J. Schneller, T.S. Sakthivel, R. Ristau, B.D. Huey, B.X.J. Yu, J.N. Jaubert, A.J. Curran, M. Wang, S. Seal, R.H. French, K.O. Davis, Characterization of front contact degradation in monocrystalline and multicrystalline silicon photovoltaic modules following damp heat exposure, Sol. Energy Mater. Sol. Cell. 235 (2022), https://doi.org/10.1016/j.solmat.2021.111468.